Journal of Applied Geophysics 123 (2015) 30–35

Contents lists available at ScienceDirect

Journal of Applied Geophysics

journal homepage: www.elsevier.com/locate/jappgeo

Joint inversion of TEM and DC in roadway advanced detection based on particle swarm optimization

Jiulong Cheng [a], Fei Li [b,*], Suping Peng [a], Xiaoyun Sun [c], Jing Zheng [a], Jizhe Jia [a]

[a] State Key Laboratory of Coal Resources and Safe Mining, China University of Mining & Technology, Beijing 100083, China
[b] Key Laboratory of Mine Disaster Prevention and Control, North China Institute of Science and Technology, Yanjiao, Beijing 101601, China
[c] School of Electrical and Electronics Engineering, Shijiazhuang Tiedao University, Shijiazhuang, 050043, China

ARTICLE INFO

Article history:
Received 18 January 2015
Received in revised form 25 July 2015
Accepted 12 September 2015
Available online 16 September 2015

Keywords:
Whole-space
Advanced detection
Transient electromagnetic method
Direct current method
Joint inversion
PSO algorithm

ABSTRACT

Transient electromagnetic method (TEM)and direct current method (DC)are two key widely applied methods for practical roadway detection, but both have their limitations. To take the advantage of each method, a synchronous nonlinear joint inversion method is proposed based on TEM and DC by using particle swarm optimization (PSO)algorithm. Firstly, a model with double low resistance anomaly and interference is constructed to test the performance of the method. Then the independent inversion and joint inversion are calculated by using the model built above. It is demonstrated that the joint inversion helped in improving the interpretation of the data to get better results. It is because that the suppression of interference and separation of the resistivity anomalies ahead and the back of the roadway working face using the proposed method. Finally, the proposed method was successfully used in a coalmine in Huainan coalfield in east China to demonstrate its practical usefulness.

© 2015 Elsevier B.V. All rights reserved.

1. Introduction

The water-bearing faults, caves, fracture and mined-out area in front of roadway/tunnel working face influence working efficiency and tunneling safety greatly in the tunneling work of mine roadway and transportation tunnels. Accurate detection of these geological anomalies is an important way to predict disasters and ensure the engineering safety.

The geophysical methods in roadway advanced detection including seismic method, transient electromagnetic method (TEM), direct current electrical method (DC), induced polarization method, ground penetrating radar (GPR)and infrared measurement of temperature etc. TEM and DC are two main methods for detecting water-bearing bodies. The research on TEM in whole space used in roadway advanced detection are no more than 10 years, and the basic theories and data processing method are immature. Besides, the anomalies ahead and the back of the roadway front overlap together and are difficult to separate, which greatly affects the practical interpretation results(Yu et al., 2007; Cheng et al., 2014a; Cheng et al., 2014b). The study of DC is focused on application instead of theory, and the detection ability is controversy(Huang et al., 2007; Han et al., 2010). TEM and DC belong to induced electrical method and conductive electrical method respectively, which makes their response characteristics different. The joint inversion using the two methods can make full use of their advantages to improve the detection precision and resolution for better results.

Joint inversion is an important method of integrated geophysical quantitative interpretation. It can be divided into joint inversion based on same physical properties and joint inversion based on different physical properties. Many researchers publish their work on joint inversion based on same physical properties (Wang, 1999; Sharma and Kaikkonen, 1999; Horspool et al., 2006; Dal Moro and Pipan, 2007; Abubakar et al., 2009). Others focus on joint inversion based on different physical properties (Colombo and Stefano, 2007; Gallardo and Meju, 2007; Moorkamp et al., 2011; Peter et al., 2012; Peng et al., 2013; Wan et al., 2013). Joint inversion of TEM and DC based on the same physical properties discussed by Raiche et al. (1985) and Yang et al. (1999). Raiche et al. (1985) accomplished 1-D joint inversion of synthetic and field TEM and DC data, showing improved interpretation of layered-earth parameters, the final model is less dependent upon starting guesses, and non-uniqueness is much less. Yang et al. (1999) carried out joint inversion of TEM and DC data to map the distributions of the freshwater/salt–water interface, presenting that the combined application of DC and TEM can make better detection maps of the freshwater/salt–water interface. All the above mentioned cases are in half space, the study of joint inversion in whole space is few. Dobroka et al. (1991)

* Corresponding author at: North China Institute of Science and Technology, Xueyuan Road, Yanjiao, Beijing, China.
E-mail address: figo1@163.com (F. Li).

http://dx.doi.org/10.1016/j.jappgeo.2015.09.008
0926-9851/© 2015 Elsevier B.V. All rights reserved.

accomplished joint inversion of VSP and DC data in a mine using 1-D 5-layer model. The test of synthetic data and field data shows it can inhibit the equivalence problem of DC, and suppress interference of seismic records.

2. Principles and algorithm of joint inversion

2.1. Complementary of TEM and DC in roadway advanced detection

TEM and DC advanced detection are complementary in the sensitivity to geological information in the front of roadway working face, the separation to geological anomalies in the front and rear, the sensitivity to conducting and resistive bodies, equivalence problem, volume effect and detection range.

DC advanced detection is less sensitive to geological information in the front of the roadway working face, but it can separate geological anomalies in front and rear, and have the same sensitivity to conducting and resistive bodies, while, TEM advanced detection is sensitive to both geological information in front and rear, but cannot separate them, and it is sensitive to conducting bodies but not to resistive bodies. The combination of two methods can provide improved interpretation to get better results.

In DC and TEM advanced detection, the response characteristics are similar when thickness and resistivity are composite values (for conducting layer it is the ratio of thickness and resistivity, for resistive layer is the product of thickness and resistivity), this equivalence problem has a great effect to inversion results. Besides, the volume effect leads to low resolution of TEM inversion results. The combination of two methods can improve detection precision and resolution by avoiding the equivalence problem and volume effect.

The detection ranges of TEM and DC are both 100 m nearby the roadway working face, and the detection blind zone of TEM is the zone where DC has a better detecting effect.

2.2. Improved particle swarm optimization

PSO is a non-liner optimization method developed in recent years, and performs well in geophysical inversion (Shi et al., 2009; Cheng et al., 2014a; Cheng et al., 2014b).

Assuming a swarm is made up of m particles, and the search space is with n dimensions, so the particle position is a n-vector. The parameters in the kth iteration can be expressed as:

The velocity of the ith particle:

$$V_i^k = \left(v_{i,1}^k, v_{i,2}^k, \ldots v_{i,j}^k, \ldots v_{i,n}^k\right) \tag{1}$$

The position of the ith particle:

$$X_i^k = \left(x_{i,1}^k, x_{i,2}^k, \ldots x_{i,j}^k, \ldots x_{i,n}^k\right) \tag{2}$$

The personal best position of the ith particle:

$$PbestX_i^k = \left(pbestx_{i,1}^k, pbestx_{i,2}^k, \ldots, pbestx_{i,j}^k, \ldots pbestx_{i,n}^k\right) \tag{3}$$

The global best position:

$$GbestX^k = \left(gbestx_1^k, gbestx_2^k, \ldots, gbestx_j^k, \ldots gbestx_n^k\right) \tag{4}$$

where, particle number $i = 1,2,\ldots\ldots,m$, iteration times $k = 1,2,\ldots\ldots,itermax$, $itermax$ is the allowable maximum iteration times.

In the beginning, initialize m particles randomly within the search space as initial value of iteration. The position of initialized particles is as Eq. (2), and the velocity is as Eq. (1). After that, particles update their velocity and position based on the following equations (Shi et al., 2009).

$$v_{i,j}^{k+1} = \omega \cdot v_{i,j}^k + c_1 \cdot r_1 \cdot \left(pbestx_{i,j}^k - x_{i,j}^k\right) + c_2 \cdot r_2 \cdot \left(gbestx_j^k - x_{i,j}^k\right) \tag{5}$$

$$x_{i,j}^{k+1} = x_{i,j}^k + v_{i,j}^{k+1} \tag{6}$$

where, j is the dimension of search space, i, k, $v_{i,j}^k, x_{i,j}^k, pbestx_{i,j}^k, gbestx_j^k$ are defined as before. c_1, and c_2 are defined as learning factors, usually, $c_1 = c_2 = 2, r_1$, and r_2 are two uniformly distributed random numbers between 0 and 1. ω is inertia factor. Eq. (5)and Eq. (6) form the basic equations of PSO algorithm. In order to improve optimization results, combined with the requirement of joint inversion, the following improvement strategies have been proposed (Cheng et al., 2014a; Cheng et al., 2014b):

$$v_{i,j}^{k+1} = \omega \cdot v_{i,j}^k + \phi_1\left(pbestx_{i,j}^k - x_{i,j}^k\right) + \phi_2\left(gbestx_j^k - pbestx_{i,j}^k\right) \tag{7}$$

Where, $\omega = 1 + \varphi_1 + \varphi_2 - \sqrt{(\varphi_1 + \varphi_2)(2 + \varphi_1 + \varphi_2)}$, $\phi_1 = c_1 \cdot rand()$, $\phi_2 = c_2\ rand()$, and $rand()$ is as random number of the range (0, 1).

Eq. (6)and (Eq. 7) form the PSO inversion algorithm in this paper.

2.3. Principles and algorithm of joint inversion

Forward modeling is the foundation of inversion. The TEM forward algorithm is discussed by paper (Krivochieva and Chouteau, 2002), and DC forward algorithm is demonstrated by paper(Ge, 1994).

A whole space 1-D upright layered model is constructed. The electricity of each layer is homogeneous and isotropic. The model includes n layers, and the thickness of the first layer and n-layer is infinite. Model parameters can be written as:

$$X = [\rho_1, \rho_2, \cdots, \rho_{n-1}, \rho_n, h_2, h_3, \cdots, h_{n-2}, h_{n-1}] \tag{8}$$

where, $\rho_1, \rho_2, \cdots, \rho_{n-1}, \rho_n$ are the resistivity of each layer. $h_2, h_3, \cdots, h_{n-2}, h_{n-1}$ are the thickness from the second layer to n − 1 layer. The total number of model parameters is 2n − 2.

Y^{TEM} is defined as forward response value of TEM advanced detection including a magnetic intensity value. f_{TEM} is defined as operator of TEM advanced detection, then TEM advanced detection forward equation can be expressed as:

$$Y_k^{TEM} = f_{TEM}(X), k = 1, 2, \cdots, a-1, a. \tag{9}$$

Y^{DC} is defined as forward response value of DC advanced detection, including b apparent resistivity value. f_{DC} is defined as operator of DC advanced detection, then DC advanced detection forward equation can be expressed as:

$$Y_k^{DC} = f_{DC}(X), k = 1, 2, \cdots, b-1, b. \tag{10}$$

In order to do synchronous joint inversion, we treat TEM advanced detection and DC advanced detection as a whole forward process. Y^{JOINT} is defined as joint forward response value of TEM and DC, including a + b response values. f_{JOINT} is defined as joint forward operator, then joint forward equation can be expressed as:

$$Y_k^{JOINT} = f_{JOINT}(X), k = 1, 2, \cdots, a+b-1, a+b \tag{11}$$

where, $f_{JOINT} = \begin{cases} f_{TEM}, 1 \le k \le a \\ f_{DC}, a < k \le a+b \end{cases}$.

The observation data of TEM advanced detection can be expressed as:

$$D^{TEM} = \left(d_1{}^{TEM}, d_2{}^{TEM}, \cdots, d_{a-1}{}^{TEM}, d_a{}^{TEM}\right) \tag{12}$$

The observation data of DC advanced detection can be expressed as:

$$D^{DC} = \left(d_1{}^{DC}, d_2{}^{DC}, \cdots, d_{b-1}{}^{DC}, d_b{}^{DC}\right) \tag{13}$$

The TEM and DC data have the same weight in joint inversion. Then the joint observation data of TEM and DC are expressed as:

$$D^{JOINT} = \left(d_1{}^{TEM}, d_2{}^{TEM}, \cdots, d_{a-1}{}^{TEM}, d_a{}^{TEM}, d_1{}^{DC}, d_2{}^{DC}, \cdots, d_{b-1}{}^{DC}, d_b{}^{DC}\right). \tag{14}$$

Simplified to:

$$D^{JOINT} = \left(d_1{}^{JOINT}, d_2{}^{JOINT}, \cdots, d_{a+b-1}{}^{JOINT}, d_{a+b}{}^{JOINT}\right). \tag{15}$$

The data misfit of joint observation data and joint forward response values is defined as:

$$\varphi = \sum_{k=1}^{a+b} \left[\left(d_k^{JOINT} - f^{JOINT}(X)\right)/d_k^{JOINT}\right]^2/(\mathrm{a}+\mathrm{b}) \tag{16}$$

Based on the data misfit, we construct joint inversion object function:

$$\Phi = \varphi. \tag{17}$$

Based on the joint forward Eq. (11), joint observation data and joint inversion object function Eq. (17), adding PSO inversion algorithm, then joint inversion of TEM and DC can be achieved.

The nonlinear joint inversion algorithm is applied to avoid the linearized process for the nonlinear problem, thus, the inversion is stable if there is no big leap between the TEM data and DC data. Besides, in the function Eq. (17), the data of DC and TEM are in the same order of magnitudes, which ensures the stability of joint inversion. Furthermore, PSO inversion algorithm only requires a proper search space instead of a definite initial model.

3. Inversion of synthetic data and analysis

3.1. Parameter setting of models

3.1.1. Parameters of PSO

More inversion model layers mean closer to real geological conditions, but increases inversion time and decreases inversion stability. Therefore, setting parameters must combine with real conditions. In this paper, a 1-D 9-layer model is chosen to inverse the theoretical model.

Model parameters are:

$$X = (\rho_1, \rho_2, \rho_3, \rho_4, \rho_5, \rho_6, \rho_7, \rho_8, \rho_9, h_2, h_3, h_4, h_5, h_6, h_7, h_8) \tag{18}$$

where, the middle of 5th layer is the roadway working face, from it to the front is the 4th layer to the 1st layer, and from it to the rear is the 6th layer to the 9th layer. $(\rho_1,\rho_2\cdots\rho_8,\rho_9)$ are the resistivity of the 1st to 9th layers, $(h_2,h_2\cdots h_6,h_8)$ are the thickness of the 2nd to 8th layers, and the thickness of the 1st and 9th layer is infinite.

Given the minimum of model parameters:

$$X_{\min} = (1,1,1,1,1,1,1,1,1,5,5,5,10,5,5,5). \tag{19}$$

Given the maximum of model parameters:

$$X_{\max} = (200,200,200,200,200,200,200,200,200,50,50,50,100,50,50,50). \tag{20}$$

3.1.2. Parameters and configuration of TEM advanced detection

By applying the central loop configuration, the transmitter and receiver are set in the middle of the 5th layer. The transmitting magnetic moment is 1 $A\cdot m^2$. Combined with field work, 60 sampling points of magnetic intensity response in the space of 10^{-5}–10^{-2} s logarithmic interval are set.

3.1.3. Parameters and configuration of DC advanced detection

The source electrode is set in the middle of the 5th layer. The electrode number is 30, the distance between adjacent electrodes is 4 m, and current is 1A.

3.2. Independent and joint inversion of a complex model with interference

A geological model is constructed consisting of 9 layers as shown in Fig. 1. Because the TEM transmitter and the DC source electrode are set in the middle layer of the model to adapt to the forward algorithms, we separate the 8th and 9th layers though they have the same resistivity. The tunneling direction is from the positive to negative direction on the x-axis, and zero stands for roadway working face. In the front of working face there are two low resistivity geological anomalies in −90–−70 m and −50–−30 m on the x-axis separately, with the same resistivity of 10 Ω·m. In the back of roadway working face (30–50 m on the x-axis) is a low resistivity geological body (with the resistivity of 50 Ω·m) and (50–80 m on the x-axis) is a high resistivity geological body (with the resistivity of 130 Ω·m). The forward data plus 5% random background interference are taken as observation data for DC inversion, TEM inversion and joint inversion separately.

Fig. 2 shows independent inversion results of TEM. Data misfit is 3.6087e-005. The inversion results are shown in Table 1. Fig. 2 shows that inversion results can reflect the existence of low resistivity

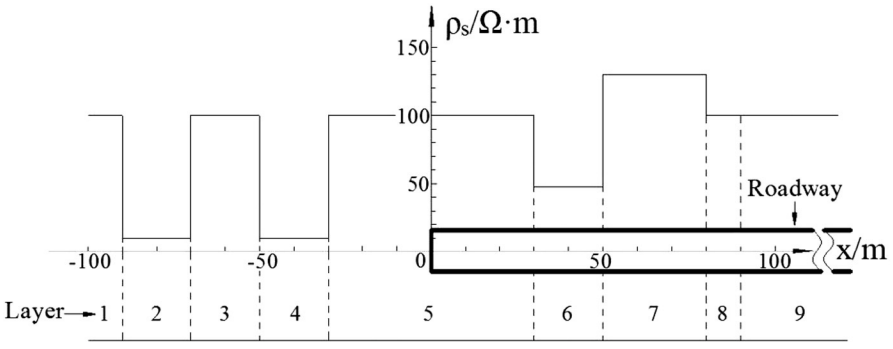

Fig. 1. Geological profile of complex model with double low resistance anomaly in front of roadway.

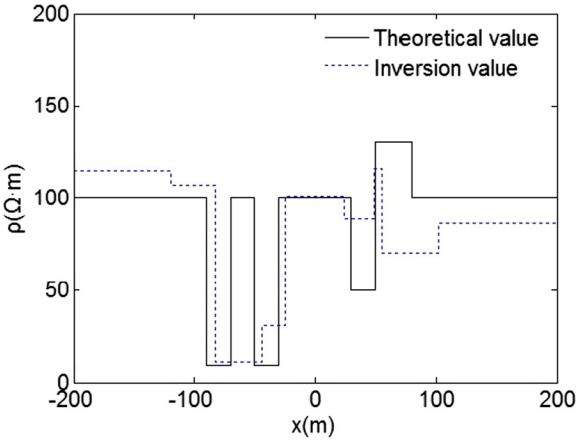

Fig. 2. Independent inversion results of TEM.

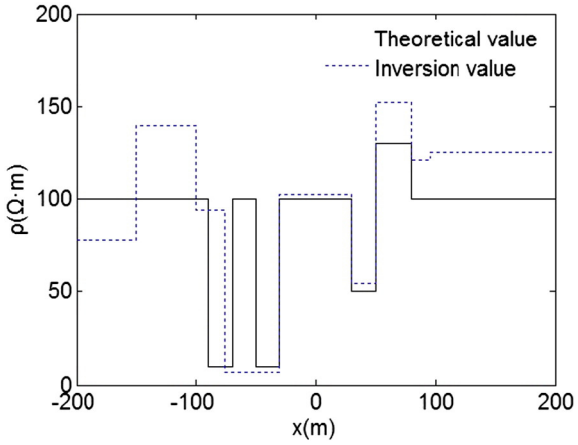

Fig. 3. Independent inversion results of DC.

anomalies in front, but the inversion result of anomalies' number, position and resistivity is bad, the equivalence problem and volume effect caused two low resistivity anomalies inversed to one big low resistivity zone. Besides, electromagnetic field is insensitive to high resistance bodies, so the inversion effect of geology in the rear is bad.

Fig. 3 shows independent inversion results of DC with the data misfit of 0.0016. Inversion results are shown in Table 1. Inversion results can reflect the existence of low resistivity anomalies, but the inversion result of anomalies' number, position, resistivity is bad, and spurious anomaly is generated in 100–150 m. It is because that the direct-current electric field is insensitive to geological information in front of the working face. Therefore, the inversion in front of the working face is comparatively dominated by TEM data in joint inversion. Besides, the inversion effect of geology in the rear is fine.

Fig. 4 is joint inversion results of model in Fig. 1 with the data misfit of 0.0076. The inversion results are shown in Table 1. Fig. 4 shows that as compared to independent inversion of TEM or DC, joint inversion achieve better detection results, the inversion result separate the two low resistivity anomalies(−90−−70 m and −50−−30 m) in front, and the inversion result of position, thickness and resistivity value seem to be in agreement with theoretical data. For low resistivity anomaly(−50−−30 m)in front, the middle position inverse error is 14.6%, thickness inverse error is 6.6%, resistivity inverse error is comparatively big (171.3%) (for the inverse error of the difference between low resistivity anomy and geological bodies nearby is low (19.0%), the interpretation can be done well). For the low resistivity in −90−−70 m, the middle position inverse error is 13.5%, thickness inverse error is 44.2%, resistivity inverse error is 8.3%. Some parameters inverse error is comparatively big because of equivalence problem and volume effect, which indicates that the joint inversion can inhibit but cannot eliminate them.

Joint inversion makes full use of the characteristic of the TEM that is sensitive to conducting bodies and the characteristic of the DC that is sensitive to geological information in the rear of the working face. By the inter-restriction and complementation of the transient electromagnetic field and the direct-current electric field, joint inversion can suppress interference, inhibit the equivalence problem and volume effect, increase the precision and resolution, and accomplish the separation of resistivity anomalies in the front and rear of roadway working face. A lot of forward modeling results demonstrate that compared with an independent inversion, joint inversion can improve the inversion precision and resolution of geological anomalies' position, thickness and resistivity significantly which leads to better detection results.

4. Field study

In a coalmine in Huainan coalfield in east China, the −700 m level central pedestrian down roadway was going to pass through the fault F10, and the fault throw of F10 is over 300 m. Affected by F10, the rock mass ruptures developed greatly. According to the geology data observed nearby roadway in the -450 m level, the affected zone of F10 is large, with a lot of small structures. The engineering geological condition is poor. Because the geological conditions in front of roadway working face is unknown, DC and TEM measurements were carried out in order to find out whether there are water-bearing geological anomalies 100 m in front of roadway working face.

DC advanced detection adopt seven electrodes configuration(Han et al., 2010), the first source electrode A is set at roadway working face, the sink electrode B is set in infinite(>400 m), the distance MN between adjacent electrodes is 7 m, and the number of measurement electrode is 14. Each time a measurement finished, the source electrode A moves back a MN distance, and measure 4 groups of electric potential value totally. Then, apparent resistivity can be calculated.

TEM advanced detection adopt central loop configuration, 2 m×2 m transmit loop, transmitter and receiver are set in roadway working face. In the horizontal plane, 11 points of data from left 50° to right 50°(at an interval of 10°) are detected.

To do joint inversion, the TEM field data along the roadway direction is chosen as the TEM observation data (Fig. 6), and the DC field data

Table 1
Inversion results of Fig. 1 model with different methods.

	ρ_1 Ω·m	ρ_2 Ω·m	ρ_3 Ω·m	ρ_4 Ω·m	ρ_5 Ω·m	ρ_6 Ω·m	ρ_7 Ω·m	ρ_8 Ω·m	ρ_9 Ω·m	h_2 m	h_3 m	h_4 m	h_5 m	h_6 m	h_7 m	h_8 m
Theoretical value	100	10	100	10	100	50	130	100	100	20	20	20	60	20	30	10
TEM inversion	115.10	107.00	11.70	30.94	100.55	88.52	116.02	70.10	86.60	36.69	38.33	19.51	49.27	24.65	6.82	45.57
DC inversion	78.25	139.71	94.32	6.64	102.23	54.19	152.42	120.53	125.58	49.75	23.59	46.53	59.99	20.19	29.61	15.63
Joint inversion	97.33	9.17	119.25	27.14	99.58	54.39	133.85	103.34	107.58	28.84	10.02	21.32	47.00	26.57	30.11	25.25

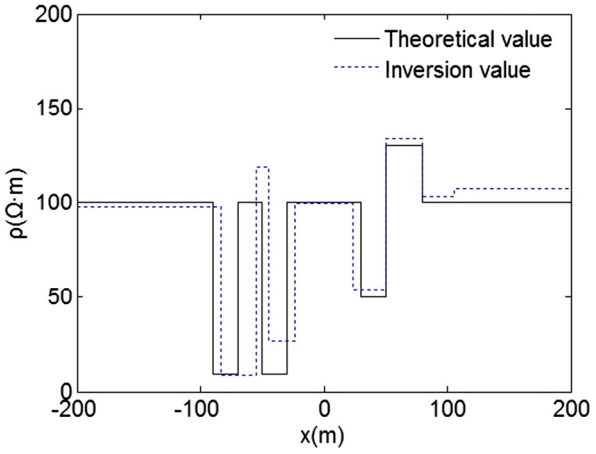

Fig. 4. Joint inversion results of Fig. 1 model.

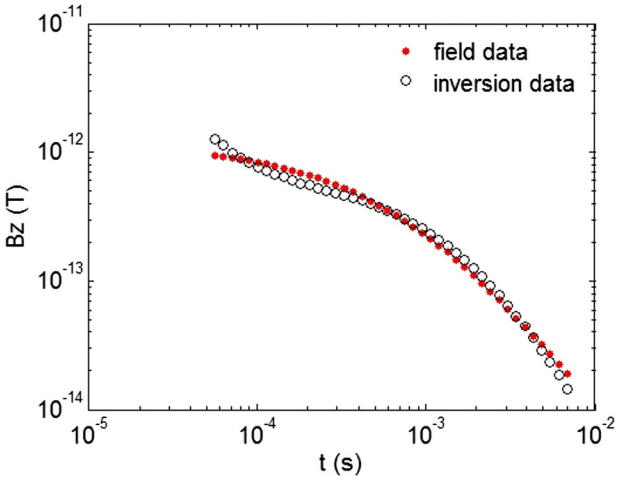

Fig. 6. Fitting of field data and inversion response (TEM).

measured by the first source electrode A at roadway working face is chosen as the DC observation data (Fig. 7). Before inversion calculation, pre-process of field data is necessary, and the observation data of TEM should normalize the transmitting magnetic moments to 1 $A \cdot m^2$. The DC observation data is carried out space correction to decrease the effect of the roadway.

Combined with the mine geological conditions, a 21-layer inversion model is constructed with parameters as follows:

$$X = (\rho_1, \rho_2, \cdots, \rho_{20}, \rho_{21}, h_2, h_3, \cdots, h_{19}, h_{20}) \quad (21)$$

where, the middle of 11th layer is the roadway working face, from it to front is the 10th layer to 1st layer, and from it to rear is the 12th layer to 21st layer. $(\rho_1, \rho_2 \cdots \rho_{20}, \rho_{21})$ are the resistivity of 1st to 21st layers, $(h_2, h_3 \cdots h_{19}, h_{20})$ are the thickness of 2nd to 20th layers, the thickness of the 1st and 21st layer are infinite. The search space of thickness of each layer is 1–20 m, and the search space of resistivity of each layer is 1–300 Ω·m.

Fig. 5 is the results of joint inversion with data misfit of 0.0245. Inversion results are shown in Table 2. Fig. 9 shows that there are two high resistivity bodies in rear of the roadway working face, and a low resistivity anomaly 25.3 m in front. The low resistivity anomalies' resistivity is 3.2 Ω·m, thickness is 6.7 m, implying a water-bearing zone existed in front of the roadway working face. The inversion results have been identified by drilling and the following tunneling work. A water-bearing fault zone was revealed 26.5 m in front of the roadway working face, with the thickness of about 8 m. The position inverse error of the fault zone is 4.53%, and it is acceptable to ensure the engineering safety.

Fig. 6 is the fitting of inverse response and field data of TEM. Fig. 7 is the fitting of inverse response and field data of DC. Fig. 6 and Fig. 7 show that the inversion model response fit well to the field data. In addition, the fitting effect is bad in the early measure time of TEM data, indicating the demerits using layered model to fit real geological conditions.

5. Discussions and conclusions

(1) Joint inversion method is applied in roadway advanced detection in the whole space, and 1-D synchronous nonlinear joint inversion algorithm of TEM and DC based on PSO is proposed and programmed. The PSO algorithm and joint inversion objective function improve the stability of inversion.

(2) Joint inversion using synthetic data and field data are calculated. The results show that compared with an independent inversion, joint inversion can improve the inversion precision and resolution in terms of anomalous zones, thickness and resistivity characteristics of target objects. It can suppress interference, inhibit the equivalence problem and volume effect, and accomplish the separation of resistivity anomalies in front and rear of roadway working face.

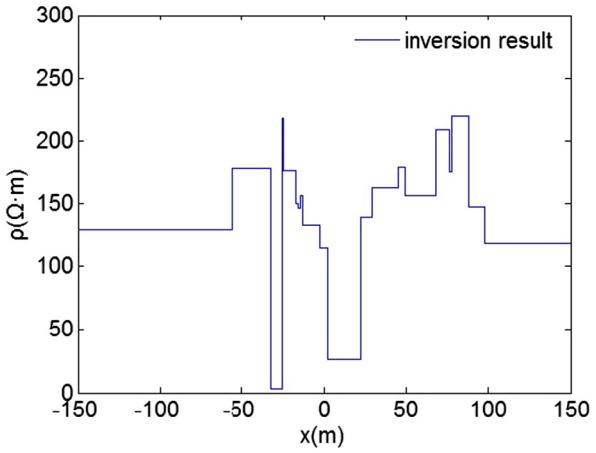

Fig. 5. Joint inversion results of field data.

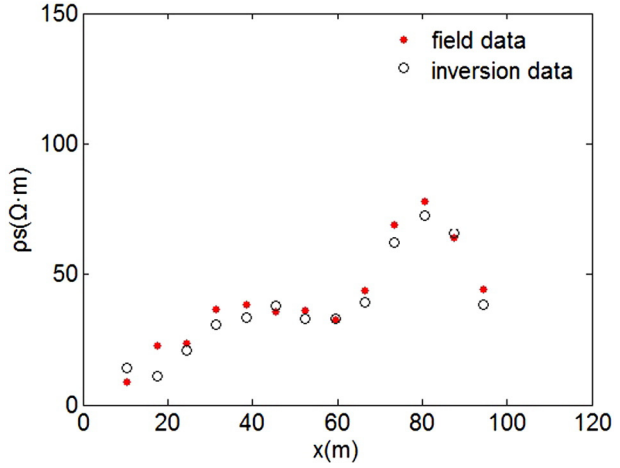

Fig. 7. Fitting of field data and inversion response (DC).

Table 2
Inversion results of field data.

Layer	1	2	3	4	5	6	7	8	9	10	11
Resistivity/Ω·m	129.14	178.38	178.26	3.22	217.89	176.38	149.89	146.60	156.42	133.14	115.12
Thickness/m	∞	16.35	8.19	6.70	1.08	7.30	1.18	1.55	1.12	10.66	4.86
Layer	12	13	14	15	16	17	18	19	20	21	
Resistivity/Ω·m	26.21	139.01	162.54	179.32	156.21	208.34	175.43	219.61	147.22	118.99	
Thickness/m	19.99	7.27	15.71	3.72	19.15	8.29	1.26	10.31	9.33	∞	

(3) In this paper, we demonstrated to address the problem by using joint inversion method. Compared with 1-D model, 2-D model approaches to real geological conditions more. Besides, the horizontally layered model are more meaningful than vertically one in the roadway advanced detection. So joint inversion based on 2-D model or horizontally layered model is the research direction in the future.

Acknowledgments

The authors would like to thank the reviewers and the editor for many helpful comments and suggestions. The research presented in this paper is supported by Natural Science Foundation of China (Grant nos. 51034003, 51174210, 51274144), Specialized Research Fund for the Doctoral Program of Higher Education (No. 20120023110014), and Chinese Universities Scientific Fund (No. 3142015019).

References

Abubakar, A., Li, M., Liu, J., et al., 2009. Simultaneous joint inversion of MT and CSEM data using a multiplicative cost function. Expanded Abstracts of 79th Annual International SEG Meeting, pp. 719–723.

Cheng, J.L., Li, F., Peng, S.P., et al., 2014a. Research progress and development direction on advanced detection in mine roadway working face using geophysical methods. J. Coal Soc. 39 (8), 1742–1750 (in Chinese).

Cheng, J.L., Li, M.X., Xiao, Y.L., et al., 2014b. Study on particle swarm optimization inversion of mine transient electromagnetic method in whole-space. Chin. J. Geophys. 57 (10), 3478–3484 (in Chinese).

Colombo, D., Stefano, M.D., 2007. Geophysical modeling via simultaneous joint inversion of seismic, gravity, and electromagnetic data: application to prestack thickness imaging. Lead. Edge 26 (3), 326–331.

Gallardo, L.A., Meju, M.A., 2007. Joint two-dimensional cross-gradient imaging of magnetotelluric and seismic travel time data for structural and lithological classification. Geophys. J. Int. 169 (3), 1261–1272.

Ge, W.Z., 1994. The forward solution of the electrical field due to a point source in layered media and its applications. Chin. J. Geophys. 37 (sup), 534–541 (in Chinese).

Han, D., Li, D., Cheng, J., et al., 2010. DC method of advanced detecting disastrous water conducting or water bearing geological structures along same layer. J. Coal Soc. 35 (4), 635–639.

Horspool, N.A., Savage, M.K., Bannister, S., 2006. Implications for intraplate volcanism and back-arcdeformation in northwestern New Zealand from joint inversion of receiver functions and surface waves. Geophys. J. Int. 166 (3), 1466–1483.

Huang, J.G., Ruan, B.Y., Wang, J.L., 2007. The fast inversion for advanced detection using DC resistivity in tunnel. Chin. J. Geophys. 50 (2), 619–624 (in Chinese).

Krivochieva, S., Chouteau, M., 2002. Whole-space modeling of a layered earth in time-domain electromagnetic measurements. J. Appl. Geophys. 50 (4), 375–391.

dobroka, M., gyulai, A., ormos, T., et al., 1991. Joint inversion of seismic and geoelectric data recorded in an underground coal mine. Geophys. Prospect. 39 (5), 643–665.

Moorkamp, M., Heincke, B., Jegen, M., et al., 2011. A framework for 3-D joint inversion of MT, gravity and seismic refraction data. Geophys. J. Int. 184 (1), 477–493.

Dal Moro, G., Pipan, M., 2007. Joint inversion of surface wave dispersion curves and reflection travel times via multi-objective evolutionary algorithms. J. Appl. Geophys. 61 (1), 56–81.

Peng, M., Tan, H.D., Jiang, M., et al., 2013. Three-dimensional joint inversion of magnetotelluric and seismic travel time data with cross gradient constraints. Chin. J. Geophys. 56 (8), 2728–2738 (in Chinese).

Peter, G.L., Colin, G.F., Charles, A.H., 2012. Joint inversion of seismic travel times and gravity data on unstructured grids with application to mineral exploration. Geophysics 77 (1), K1–K15.

Raiche, A.P., Jupp, D.L.B., Rutter, H., et al., 1985. The joint use of coincident loop transient electromagnetic and schlumberger sounding to resolve layered structures. Geophysics 50 (10), 1618–2627.

Shi, X.M., Xiao, M., Fan, J.K., et al., 2009. The damped PSO algorithm and its application for magnetoelluric sounding data inversion. Chin. J. Geophys. 52 (4), 1114–1120 (in Chinese).

Sharma, S.P., Kaikkonen, P., 1999. Appraisal of equivalence and suppression problems in 1D EM and DC measurements using global optimization and joint inversion. Geophys. Prospect. 47 (2), 219–249.

Wang, Y.H., 1999. Simultaneous inversion for model geometry and elastic parameters. Geophysics 64 (1), 182–190.

Wan, L., Lin, T.T., Lin, J., et al., 2013. Joint inversion of MRS and TEM data based on adaptive genetic algorithm. Chin. J. Geophys. 56 (11), 3728–3740 (in Chinese).

Yang, C.H., Tong, L.T., Huang, C.F., 1999. Combined application of DC and TEM to sea-water intrusion mapping. Geophysics 64 (2), 417–425.

Yu, J.C., Liu, Z.X., Liu, S.C., 2007. Theoretical analysis of mine transient electromagnetic method and its application in detecting water burst structures in deep coal stope. J. Coal Soc, (8), 818–821 (in Chinese).